



Contents lists available at ScienceDirect

## Thin Solid Films

journal homepage: [www.elsevier.com/locate/tsf](http://www.elsevier.com/locate/tsf)

## Optimization of thermoelectric properties on Bi<sub>2</sub>Te<sub>3</sub> thin films deposited by thermal co-evaporation

L.M. Goncalves<sup>a,\*</sup>, C. Couto<sup>a</sup>, P. Alpuim<sup>b</sup>, A.G. Rolo<sup>b</sup>, F. Völklein<sup>c</sup>, J.H. Correia<sup>a</sup>

<sup>a</sup> University of Minho, Dept. of Industrial Electronics, Azurem, 4800-058 Guimaraes, Portugal

<sup>b</sup> University of Minho, Dept. of Physics, Azurem, 4800-058 Guimaraes, Portugal

<sup>c</sup> University of Applied Sciences Wiesbaden, Am Bruckweg 26, Russelsheim, Germany

## ARTICLE INFO

Available online xxxx

## Keywords:

Thermoelectric properties

Thin films

Peltier micro-cooler

Thermopile

Bismuth telluride

Flexible substrate

Polyimide

## ABSTRACT

The optimization of the thermal co-evaporation deposition process for n-type bismuth telluride (Bi<sub>2</sub>Te<sub>3</sub>) thin films deposited onto polyimide substrates and intended for thermoelectric applications is reported. The influence of deposition parameters (evaporation rate and substrate temperature) on film composition and thermoelectric properties was studied for optimal thermoelectric performance. Energy-dispersive X-ray spectroscopy, X-ray diffraction, X-ray photoelectron spectroscopy and Raman spectroscopy confirmed the formation of Bi<sub>2</sub>Te<sub>3</sub> thin films. Seebeck coefficient (up to 250 μV K<sup>-1</sup>), in-plane electrical resistivity (≈10 μΩ m), carrier concentration (3×10<sup>19</sup>–20×10<sup>19</sup> cm<sup>-3</sup>) and Hall mobility (80–170 cm<sup>2</sup>V<sup>-1</sup>s<sup>-1</sup>) were measured at room temperature for selected Bi<sub>2</sub>Te<sub>3</sub> samples.

© 2009 Elsevier B.V. All rights reserved.

### 1. Introduction

Integration of efficient solid state thermoelectric microdevices with microelectronics is desirable for both local cooling and thermoelectric microgeneration. Tellurium alloys (n-type Bi<sub>2</sub>Te<sub>3</sub> and p-type Sb<sub>2</sub>Te<sub>3</sub>) are well-established room-temperature thermoelectric materials that are widely used in the thermoelectric industry due to their high Seebeck coefficient, low electrical resistivity and relatively low thermal conductivity [1].

In the present work thin-film planar technology was chosen in order to scale down conventional bulk thermoelectric devices to the micron size range. Thin-film technology allows for an enlarged choice of the type of substrate, for the possibility of patterning the devices to micro or sub-micro dimensions and for easy integration with standard Si technology [2,3]. In this paper, the possibility of integration with next-generation flexible electronic devices will also be demonstrated.

Several deposition techniques have been reported in the literature for the fabrication of Bi<sub>2</sub>Te<sub>3</sub> thin films: co-sputtering, electrochemical deposition, metal-organic chemical vapor deposition and flash evaporation, are some examples. Zou et al. [4] fabricated n-type and p-type Bi<sub>2</sub>Te<sub>3</sub> films and showed the influence of substrate temperature and evaporation rate on the electronic properties of the deposited films. Their work was based on a small number of samples, and no consistent relation could be established between deposition conditions and material performance. Silva et al. [5] more recently reported the fabrication

of co-evaporated thermoelectric Bi<sub>2</sub>Te<sub>3</sub> thin films in silicon substrates. Optimal deposition temperature could not be achieved, however, because of limitations in the patterning process. Kim et al. showed the influence of substrate temperature on the properties of Bi<sub>2</sub>Te<sub>3</sub> thin films deposited by co-sputtering [6] and Böttner fabricated thermoelectric devices using a two wafer process [7].

Thermal evaporation is an attractive technique because of its relative simplicity, ease of process control and scalability to large areas and high throughput. However, our previous results [8] show that direct evaporation of the bulk material (Bi<sub>2</sub>Te<sub>3</sub>) results in a compositional gradient through the film thickness due to the large difference in the vapor pressures of bismuth and tellurium. Thermal co-evaporation of pure Bi and Te is used instead since it allows independent control of the temperature and consequently of the partial vapor pressures of both components. In the present work, the influence of deposition parameters (evaporation rates of Bi and Te and substrate temperature) is studied in detail and more than 100 samples were fabricated to allow a consistent correlation to be established between the growth conditions and the thermoelectric properties of the films. Glass, silicon and polyimide (Kapton<sup>®</sup>) were investigated as substrates, with good adhesion to the film in all cases. However, 25 μm-thick polyimide film was finally chosen as a substrate because of its low thermal conductivity (0.12 Wm<sup>-1</sup>K<sup>-1</sup>) and because the value of its thermal expansion coefficient (12×10<sup>-6</sup>K<sup>-1</sup>) closely matches the thermal expansion coefficient of the telluride films, thus reducing residual stress and increasing adhesion. Moreover, flexible substrates add uncommon mechanical properties to the composite film-substrate, enabling their integration with many types of devices [9].

\* Corresponding author. Tel.: +351 253510190; fax: +351 253510189.  
E-mail address: [lgoncalves@dei.uminho.pt](mailto:lgoncalves@dei.uminho.pt) (L.M. Goncalves).

$\text{Bi}_2\text{Te}_3$  is a semiconductor with a 0.150 eV energy gap [10] and a rhombohedral unit cell belonging to space group  $R\bar{3}m$  ( $D_{3d}^5$ ). Experimental results for the Raman active modes observed in  $\text{Bi}_2\text{Te}_3$  films are presented in this work and compared to results relating to bulk crystals presented in the literature.

## 2. Experimental details

Bismuth telluride films were fabricated using the thermal co-evaporation technique in a high-vacuum chamber with base pressure  $p = 3 \times 10^{-6}$  mbar. The power applied to each boat was controlled independently, using two PID (Proportional Integral and Derivative) controllers in order to maintain the deposition rate at a fixed value, different for each material. The Bi evaporation flow rate ( $F_{\text{rBi}}$ ) was maintained at  $2 \text{ \AA s}^{-1}$ , and the Te evaporation flow rate ( $F_{\text{rTe}}$ ) was varied in the range  $3\text{--}9 \text{ \AA s}^{-1}$ . The evaporation flow rate ratio,  $R$  ( $R = F_{\text{rTe}}/F_{\text{rBi}}$ ), is defined as the number of atoms of Te divided by the number of atoms of Bi that arrive in unit time at the substrate during deposition.

Each PID controller reads the deposition rate from a thickness monitor and is designed to compute in real-time the power necessary to be applied to the corresponding evaporation boat in order to achieve the user-defined constant evaporation rate. Each thickness monitor, consisting of a quartz crystal oscillator, is carefully placed inside the chamber in order to receive material only from the boat it is expected to monitor. The measured thickness and deposition rate depend on the physical position of the sensor, the material density and the usage of the sensor. The measurement system was calibrated by depositing a  $1 \mu\text{m}$  thick film of  $\text{Bi}_2\text{Te}_3$  and subsequently verifying the thickness by SEM imaging, for different substrate positions. Although the deposition rate was corrected for each substrate position, an error of up to 10% is estimated. A metal sheet was placed between the two boats to partially separate the flows from the two evaporants, fully preventing mixing of both materials at the quartz crystals. Large boats (baffled boxes,  $4 \text{ cm}^3$  volume) were used, in order to maintain stable evaporation rates during the deposition time. Substrates were heated to the temperature set point ( $T_{\text{sub}}$ ) in the range between  $150 \text{ }^\circ\text{C}$  and  $300 \text{ }^\circ\text{C}$ . Substrate temperature was measured in the aluminum substrate holder, as close as possible to the substrate. However, the temperature on the polyimide surface was lower than the measured value due to the low thermal conductivity of polyimide, to the thermal inertia of the system and to radiation losses.

SEM images of the sample surface and cross-section were taken. The chemical composition of the film and its structure were studied by Energy-Dispersive X-ray spectroscopy (EDX), by X-ray diffraction (XRD) using copper  $K_\alpha$  radiation ( $\lambda = 1.54051 \text{ \AA}$ ), by X-ray photoelectron spectroscopy (XPS) with equipment VG SCIENTIFIC model Escalab 250iXL, and by Raman spectroscopy. For selected films the composition was confirmed by Rutherford Backscattering Spectroscopy (RBS) [13] and Particle Induced X-ray Emission (PIXE). For Raman scattering experiments, both the  $514.5 \text{ nm}$  and  $488 \text{ nm}$  lines of an Ar+ laser and the  $1064 \text{ nm}$  line of an YAG:Nd laser were used for excitation. Raman spectra were obtained from the above-stated first two visible lines in a Jobin-Yvon T64000 spectrometer (micro-Raman, in the  $30\text{--}700 \text{ cm}^{-1}$  Raman shift range, with spot size  $\sim 1 \mu\text{m}$  and spectral resolution  $\sim 1 \text{ cm}^{-1}$ ) and from the third infrared line in a Bruker RFS 100/S FT-Raman spectrometer (macro-Raman,  $50\text{--}2000 \text{ cm}^{-1}$  Raman shift range, spot size  $\sim 100 \mu\text{m}$  and spectral resolution  $\sim 2 \text{ cm}^{-1}$ ). In all cases, Raman spectra were recorded at room temperature, in a backscattering geometry with polarized incident light and without analyser.

In-plane electrical resistivity, carrier concentration and Hall mobility were measured at room temperature using the conventional four probe van der Pauw geometry in a  $5 \text{ mm}$  side square arrangement. A DC magnetic field of  $80 \text{ mT}$  was applied for Hall measurements. The

Seebeck coefficient,  $\alpha$ , was measured by connecting one side of the film to a heated metal block at a fixed temperature and the other side to a heat sink kept at room temperature, with a temperature difference between both sides below  $10 \text{ }^\circ\text{C}$ . Thermal conductivity was measured using the technique developed in [11]. An additional film of BiSb was deposited onto the bottom side of the substrate. Current was applied through this film, and heating was measured indirectly by monitoring the resistivity change in this material. Using the value of applied power, the unknown thermal conductivity of the thermoelectric film was calculated. Power factor (PF) was calculated using eq. 1 and the dimensionless parameter *figure of merit* (ZT) was obtained from Eq. (2) ( $\alpha$  is in  $\text{V K}^{-1}$ ,  $\rho$  is electrical resistivity in  $\Omega \text{ m}$ ,  $\lambda$  is the thermal conductivity in  $\text{W m}^{-1} \text{K}^{-1}$  and  $T$  is the temperature in K). An error below 10% is expected in ZT values.

$$PF = \alpha^2 / \rho \quad (1)$$

$$ZT = \frac{\alpha^2}{\rho\lambda} T \quad (2)$$

## 3. Results and discussion

A series of  $\text{Bi}_2\text{Te}_3$  films was deposited at different flow rate ratio,  $R$ , and substrate temperature,  $T_{\text{sub}}$ , in order to study the effect of these parameters on the thermoelectric properties.  $R$  was set by fixing the Bi evaporation flow rate ( $F_{\text{rBi}}$ ) at  $2 \text{ \AA s}^{-1}$  and varying the Te evaporation flow rate ( $F_{\text{rTe}}$ ) in the range  $3\text{--}9 \text{ \AA s}^{-1}$ . An error of  $\pm 10\%$  should be considered for data associated with the evaporation rate measurements, due to the uncertainties in the positioning of the sensors and in the densities of the materials. Three series of films were fabricated, at  $T_{\text{sub}} = 190, 230$  and  $270 \text{ }^\circ\text{C}$ . All films were  $\sim 1 \mu\text{m}$  thick ( $\pm 30\%$ ). Table 1 summarizes the thermoelectric properties of selected  $\text{Bi}_2\text{Te}_3$  films.

XRD interferograms (Fig. 1) reveal the polycrystalline structure of the films. The powder diffraction spectra for polycrystalline  $\text{Bi}_2\text{Te}_3$  are also represented in Fig. 1, as dashed lines. Table 2 summarizes the main planes detected in each film and the corresponding crystalline phases (card 15-863 and card 22.715 from [12]). The observed XRD peaks agree well with the powder diffraction spectra for polycrystalline  $\text{Bi}_2\text{Te}_3$  (card 15-863 from [12]), or  $\text{Bi}_{0.43}\text{Te}_{0.57}$  (card 22.715 from [12]). Similar XRD results obtained from thin-film material can be found in the literature [5,6]. The difference in XRD patterns for the two films analyzed is explained by the different substrate temperature used in each case. The tellurium atomic content is 59% for film #282 and 55.5% for film #302 as determined by EDX. Film #282 was deposited at  $T_{\text{sub}} = 240 \text{ }^\circ\text{C}$  and film #302 at  $T_{\text{sub}} = 160 \text{ }^\circ\text{C}$ . No significant peaks could be found corresponding to those of the BiTe phase (card 44-667), contrary to what is found in literature for co-sputtered  $\text{Bi}_2\text{Te}_3$  [6]. The SEM cross-sectional and surface images of the films confirm their polycrystalline structure. The effect of substrate temperature on polycrystalline morphology can be seen in

**Table 1**  
Properties of selected  $\text{Bi}_2\text{Te}_3$  films.

Film	Temp $T_{\text{sub}}$ , $^\circ\text{C}$	$R = F_{\text{rTe}}/F_{\text{rBi}}$	%Te by EDX	$\alpha$ , $\mu\text{V K}^{-1}$	$\rho$ , $\Omega \text{ m}$	$PF \times 10^{-3}$ , $\text{W K}^{-2} \text{ m}^{-1}$
#302A	160	1.6	55.5%	-74	5.7	0.96
#187A	190	1.5	-	-62	5.7	0.67
#C36	190	1.7	-	-180	16.6	1.95
#267A	230	2.1	62.8%	-156	11.3	2.16
#267D	230	3.0	62.2%	-152	13.4	1.72
#282B	240	3.2	59.1%	-180	7.3	4.44
#273C	270	3.2	62.0%	-248	12.6	4.87
#281D	270	3.9	-	-220	10.6	4.57

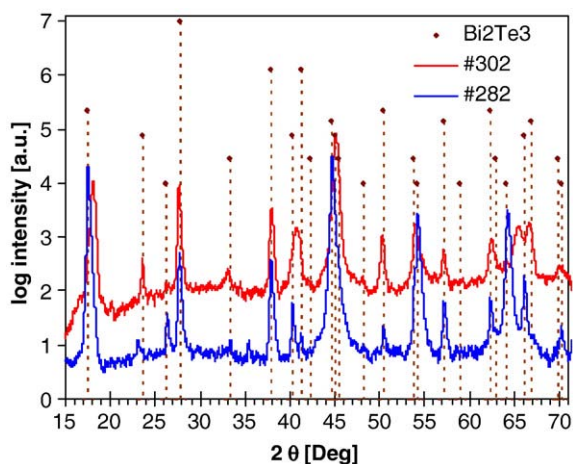


Fig. 1. XRD diffractograms of films #302 and #282 deposited at substrate temperatures of 160 °C and 240 °C respectively.

Fig. 2. Lower full width at half maximum (FWHM) of XRD peaks in films deposited at higher  $T_{\text{sub}}$  indicate the existence of larger grains than in those deposited at lower  $T_{\text{sub}}$ . Using Scherrer formula, grain sizes larger than 500 nm were found in films deposited at a substrate temperature of 240 °C (Fig. 2-A) and smaller grains (200 nm) in films deposited at 160 °C (Fig. 2-B). In general, the grain size of co-evaporated  $\text{Bi}_2\text{Te}_3$  was observed to increase with substrate temperature. This effect can be explained by higher surface mobility and clustering of adatoms when more thermal energy is available during film growth.

Bulk  $\text{Bi}_2\text{Te}_3$  is a semiconductor which at room temperature belongs to the space group  $R\bar{3}m$  ( $D_{3d}^5$ ) [10] and presents four Raman active modes. Three Raman modes of  $\text{Bi}_2\text{Te}_3$  were detected in our films. We were not able to detect any peak at wavenumbers lower than  $60\text{ cm}^{-1}$ . However, the lowest wavenumber Eg-mode, predicted at  $50.6\text{ cm}^{-1}$  [14] has already been measured, although with very low intensity, at  $36.5\text{ cm}^{-1}$  [see Ref. 10]. Fig. 3 shows Raman spectra of the  $\text{Bi}_2\text{Te}_3$  films obtained using different excitation energies. The frequencies of the modes and the full width at half maximum of each peak were determined by fitting a Lorentzian function to each peak. The fitting parameters are shown in Table 3 together with the calculated and experimental bulk frequencies reported in the literature [10,14,15]. In a set of selected films no significant frequency changes were noticed in Raman shifts as the excitation wavelength was changed from 1064 nm to 514.5 nm and to 488 nm. Also no significant deviations from the

Table 2

XRD planes detected in films #302 and #282 deposited at substrate temperatures of 160 °C and 240 °C respectively and reference values from [12].

Material	BulkI (a.u)	Plane	2θ	#282I (a.u)	#302I (a.u)
$\text{Bi}_2\text{Te}_3$	8	0 0 6	17.45	70	4
$\text{Bi}_{0.43}\text{Te}_{0.57}$	65	0 0 11	17.94		20
$\text{Bi}_{0.43}\text{Te}_{0.57}$	4	1 0 2	23.51		4
$\text{Bi}_{0.43}\text{Te}_{0.57}$	25	0 1 9	27.59		30
$\text{Bi}_2\text{Te}_3$	100	0 1 5	27.66	1.5	
$\text{Bi}_2\text{Te}_3$	25	1 0 10	37.83	1.1	8
$\text{Bi}_{0.43}\text{Te}_{0.57}$	35	1 0 18	37.98		8
$\text{Bi}_2\text{Te}_3$	4	0 1 11	40.26	0.2	
$\text{Bi}_2\text{Te}_3$	6	0 0 15	44.57	100	
$\text{Bi}_2\text{Te}_3$	4	1 1 6	44.99		60
$\text{Bi}_{0.43}\text{Te}_{0.57}$	100	0 0 27	45.02		60
$\text{Bi}_2\text{Te}_3$	2	0 0 16	53.82		6
$\text{Bi}_{0.43}\text{Te}_{0.57}$	10	0 0 32	53.95		6
$\text{Bi}_2\text{Te}_3$	6	0 2 10	57.13	8	
$\text{Bi}_2\text{Te}_3$	8	1 1 15	62.25	1	
$\text{Bi}_{0.43}\text{Te}_{0.57}$	15	1 1 27	62.39		4
$\text{Bi}_2\text{Te}_3$	4	0 1 20	66.01	0.5	

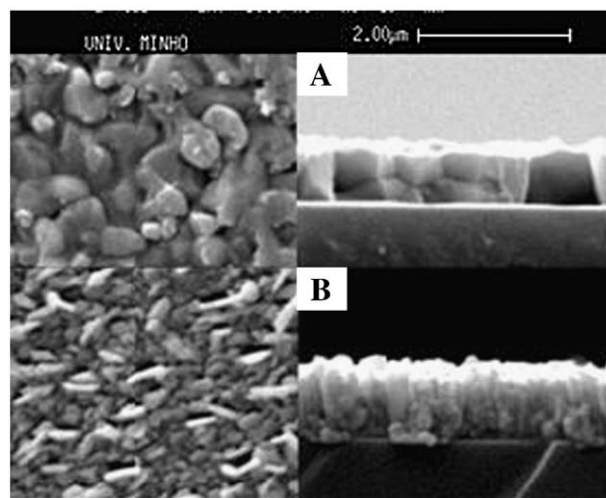


Fig. 2. (A and B): Surface and cross-sectional SEM images of  $\text{Bi}_2\text{Te}_3$  films deposited on glass at (A)  $T_{\text{sub}} = 240\text{ °C}$  and  $R = 3.2$  and (B)  $T_{\text{sub}} = 160\text{ °C}$  and  $R = 1.6$ .

Raman shifts found for the bulk material (see Fig. 3) were detected for the analysed films as the peak frequencies agree well with those found in the literature for calculated [14] and experimental [10,15] Raman bulk active modes. The peak at  $\sim 200\text{ cm}^{-1}$  is present in the spectra of both bulk (using 488 nm excitation) and film (using 488 nm and 514.5 nm excitations) materials, though with different intensity relatively to the Eg peak. It may very likely be an overtone of the Eg mode at  $\sim 100\text{ cm}^{-1}$ . Additional studies are necessary in order to further clarify the nature of this peak.

Fig. 4 shows the atomic percent tellurium content in the films plotted against the evaporated tellurium, in the same units. Since the atomic Te percentage incorporated in the films is always smaller than the corresponding percentage of evaporated Te and depends on substrate temperature, the evaporation rate of tellurium must be adjusted to overcome these factors, and obtain the desired stoichiometry. This effect is more noticeable as  $T_{\text{sub}}$  increases. Since, at 300 °C, the vapor pressure of Te is  $10^5$  higher than the vapor pressure of Bi, it is possible to explain the effect by re-evaporation of Te from the heated substrate is at a much higher rate than Bi. This explains why it is necessary to use a higher value of  $R$  than the desired atomic ratio of Te/Bi in the final film composition (60%Te/40%Bi). XPS measurements revealed that contamination with carbon and oxygen occurred only at the film surface.

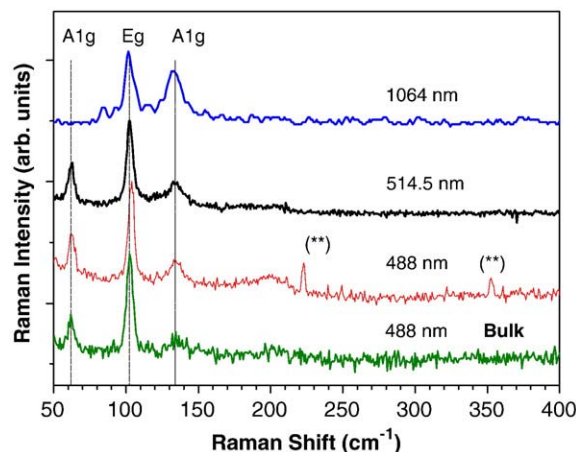


Fig. 3. Typical Raman spectra obtained from a  $\text{Bi}_2\text{Te}_3$  film at room temperature with different excitation laser lines ( $\lambda = 1064\text{ nm}$ ,  $514.5\text{ nm}$  and  $488\text{ nm}$ ) and that of the bulk for comparison. The symbol (\*\*) marks laser lines.

**Table 3**  
Frequencies and FWHM of Raman peaks for the Bi<sub>2</sub>Te<sub>3</sub> films obtained with different excitation lines.

Modes Bi <sub>2</sub> Te <sub>3</sub>	Our work λ = 1064 nm		Our work λ = 514.5 nm		Our work λ = 488 nm		Calc.[14]	Exp.[15]	Exp.[10]
	Freq.(cm <sup>-1</sup> )	FWHM(cm <sup>-1</sup> )	Freq.(cm <sup>-1</sup> )	FWHM(cm <sup>-1</sup> )	Freq.(cm <sup>-1</sup> )	FWHM(cm <sup>-1</sup> )	Freq.(cm <sup>-1</sup> )	Freq.(cm <sup>-1</sup> )	Freq.(cm <sup>-1</sup> )
E <sub>g</sub> <sup>1</sup>	-	-	-	-	-	-	50.6	-	36.5
A <sub>1g</sub> <sup>1</sup>	-	-	62.3	4.7	62.3	5.0	71.1	62.5	62.0
E <sub>g</sub> <sup>2</sup>	102.1	7.6	102.7	5.6	103.7	5.0	118.5	103.0	102.3
A <sub>1g</sub> <sup>2</sup>	133.8	14.9	134.0	11.5	134.2	12.5	128.3	134.0	134.0

For comparison the calculated and experimental frequencies from the literature are also presented.

Fig. 5 shows the dependence of the Seebeck coefficient, electrical resistivity, carrier concentration and power factor on the flow rate ratio (*R*), for films deposited at different substrate temperatures (190, 230 and 270 °C). At each *T*<sub>sub</sub> the maximum absolute value of the Seebeck coefficient is obtained at a value of *R* that depends on *T*<sub>sub</sub>. It is evident from the negative signs of both Seebeck and Hall coefficients that the majority carriers in Bi<sub>2</sub>Te<sub>3</sub> films are electrons. Films with compositions in Te richer than stoichiometric have lower carrier concentration (<10<sup>20</sup> cm<sup>-3</sup>), higher mobility (>50 cm<sup>2</sup>V<sup>-1</sup>s<sup>-1</sup>), and higher Seebeck coefficient, leading to a higher power factor. Films obtained with *R* < 1.2 are Bi-rich and have high carrier concentration. This results in a decreased value of power factor.

If one considers the information conveyed by Fig. 5, one concludes that, taking the results of series for all temperatures, a high power factor correlates with a high absolute value of Seebeck coefficient, with a low carrier concentration, and with a relatively high electrical resistivity. It is no surprise that the value of the Seebeck coefficient determines the hierarchy of the Bi<sub>2</sub>Te<sub>3</sub> films in the PF scale, given the quadratic dependence of PF in α, as is clear in Eq. (1). But Eq. (1) also predicts a linear increase in PF with electrical conductivity, when keeping other parameters constant. Since the observed PFs dramatically decrease as the carrier concentration and electrical conductivity increase, one is forced to conclude that these increments are the result of major changes in the band structure and position of the Fermi level in the density of states (DOS). These changes are also responsible for the observed decrease in α. In fact, according to the Mott theory of the Seebeck coefficient [16], α critically depends on the derivative with respect to the energy of the DOS at the Fermi energy.

At each *T*<sub>sub</sub> the maximum value of PF is obtained at a value of *R* that depends on *T*<sub>sub</sub>. Maximum PF is obtained at *R* = 2, 2.5 and 3.5 respectively for *T*<sub>sub</sub> = 190, 230 and 270 °C. The influence of substrate temperature on power factor is shown in Fig. 6. Results from literature

are also shown [4,5] for comparison. The best films were obtained at *T*<sub>sub</sub> = 270 °C. For *T*<sub>sub</sub> > 290 °C films with high mechanical stress and/or poor adhesion were obtained due to the degradation of the polyimide substrate. A thermoelectric *PF* = 4.9 × 10<sup>-3</sup> WK<sup>-2</sup> m<sup>-1</sup> was obtained for films deposited at *T*<sub>sub</sub> = 270 °C with Bi evaporation rate of 2 Ås<sup>-1</sup> and Te evaporation rate of 6.4 Ås<sup>-1</sup> (*R* = 3.2). These evaporation parameters resulted in a near-stoichiometric composition (by EDX analysis) of the material with 35–40% of Bi and 65–60% of Te. Higher substrate temperature leads to higher absolute value of Seebeck coefficient and to lower resistivity (when *R* is adjusted to obtain near-stoichiometric films), as can be seen in Fig. 5. Higher thermoelectric quality is promoted by larger grain sizes. For substrate temperatures above 290 °C the deposition of stoichiometric films is very difficult, since an extremely high *R* is required to compensate the re-evaporation of tellurium from the substrate. But this temperature range is incompatible with the use of polyimide substrates and therefore was not investigated further. Fig. 6 also shows that, for all substrate temperatures, films with higher power factor are obtained when the composition is slightly tellurium rich (60–65%). Equivalent results (also shown in Fig. 6) were found in literature for thin-films [5] and bulk single crystals [17].

Spatial uniformity of the Seebeck coefficient was evaluated in 40 μm × 40 μm spots, along a 5 mm × 5 mm area, as shown in Fig. 7. A heated probe was placed in successive positions on the film in order to measure the Seebeck coefficient over the entire surface area [18]. The Seebeck coefficient varies from -120 μV K<sup>-1</sup> to -220 μV K<sup>-1</sup> on this surface. This non-uniformity is due to deficient thermal contact between substrate and heater (which causes temperature gradients in the film during deposition) and absence of rotation of the substrate. Therefore, a similar variation is expected in other electronic properties of the films.

Thermal conductivity (*κ*) was measured on Bi<sub>2</sub>Te<sub>3</sub> films and a value of 1.3 Wm<sup>-1</sup>K<sup>-1</sup> was obtained at room temperature (see Fig. 8). Thermal conductivity is due to electron and phonon contributions, respectively *κ*<sub>e</sub> and *κ*<sub>p</sub>, and *κ* = *κ*<sub>e</sub> + *κ*<sub>p</sub>. Electron contribution was estimated using Wiedemann–Franz law, *κ*<sub>e</sub> = *LT*/ρ<sub>e</sub>, where *L* is the Lorenz number, *T* the temperature and ρ<sub>e</sub> is the electrical resistivity. Considering *L* = 1.5 × 10<sup>-8</sup> V<sup>2</sup>K<sup>-2</sup> at 300 K [19], *κ*<sub>e</sub> = 0.45 Wm<sup>-1</sup>K<sup>-1</sup> is obtained (for a resistivity of 10 μΩ m) and *κ*<sub>p</sub> = 0.85 Wm<sup>-1</sup>K<sup>-1</sup>. Using these values, a figure of merit (*ZT*) near unity is obtained for the best Bi<sub>2</sub>Te<sub>3</sub> thin films.

The errors arising from deposition rate and substrate temperature measurements, and non-uniformity of properties in the film surface (the measurement area on the film is not the same for all measurements) could justify the large spread in the data presented. However, the relationship between deposition parameters and the thermoelectric properties of Bi<sub>2</sub>Te<sub>3</sub> thin films was established satisfactorily in this work.

**4. Conclusions**

N-type Bi<sub>2</sub>Te<sub>3</sub> thermoelectric thin films with high figures of merit were fabricated by thermal co-evaporation. The optimized films have a power factor of 4.87 × 10<sup>-3</sup> WK<sup>-2</sup> m<sup>-1</sup>, comparable with the best results found in literature for the same material. Films were deposited

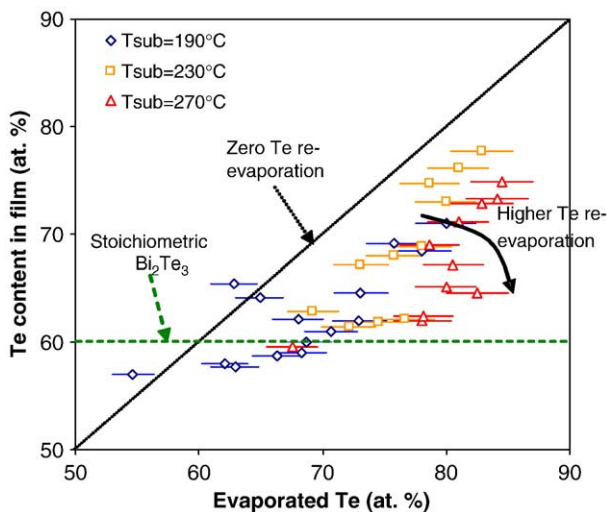


Fig. 4. Atomic percent tellurium content in the films plotted against the atomic percent of evaporated tellurium.

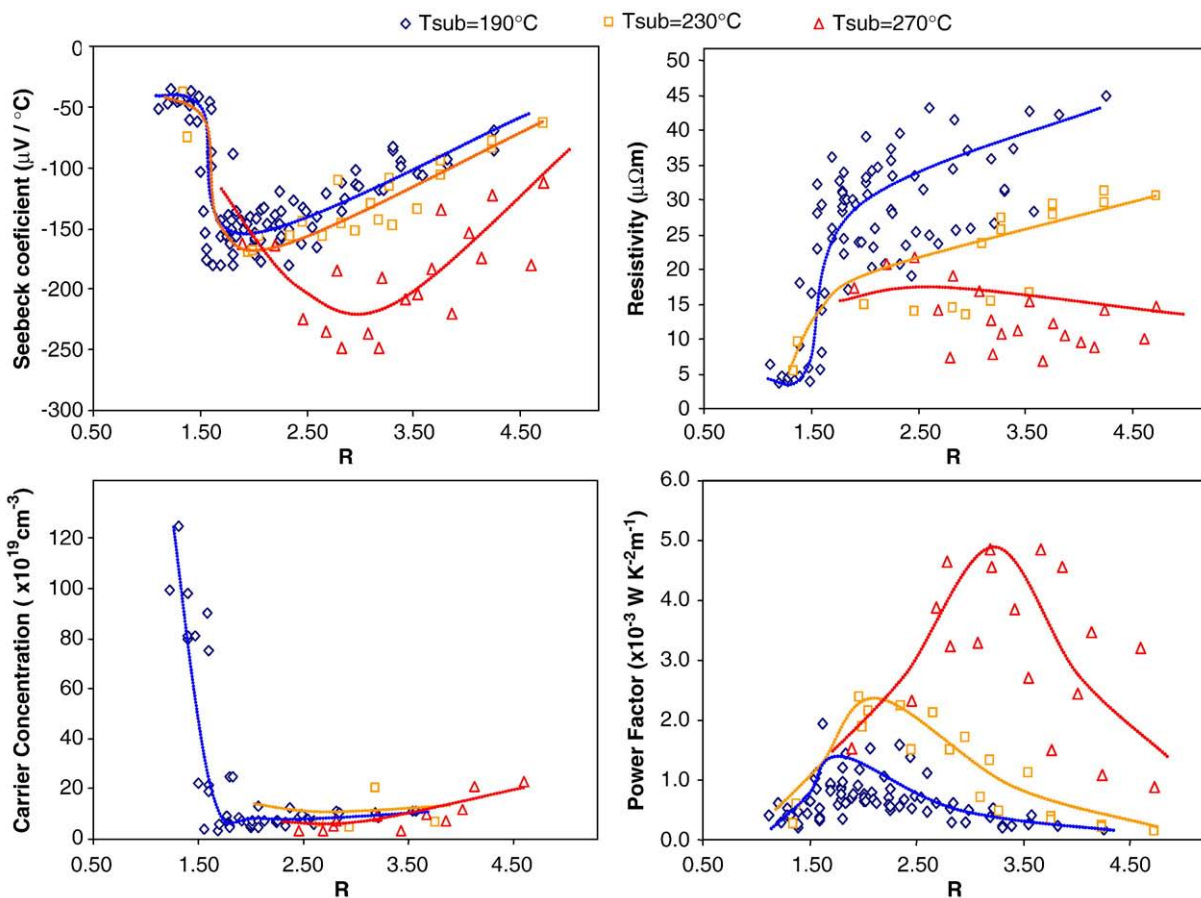


Fig. 5. Seebeck coefficient, electrical resistivity, carrier concentration and power factor of  $\text{Bi}_2\text{Te}_3$  thin films as a function of Te/Bi evaporation flow ratio,  $R$  (lines are guides to the eye).

onto glass and flexible polyimide substrates, with good adhesion. The influence of evaporation rates and substrate temperature on composition, Seebeck coefficient, electrical resistivity, and carrier concentration is reported. Using EDX results it is shown that films with high power factors are obtained when their composition is nearly stoichiometric (35–40% Bi, 65–60% Te). The highest thermoelectric power factor is obtained at a substrate temperature  $\sim 270^\circ\text{C}$ . Bi and Te

evaporation rates were  $2\text{ \AA s}^{-1}$  and  $6.4\text{ \AA s}^{-1}$ , respectively, for this sample. For all substrate temperatures the highest power factors are obtained for samples that show the highest values of Seebeck coefficient. Thermal conductivity of  $1.3\text{ W m}^{-1}\text{K}^{-1}$  is measured and a *figure of merit* close to unity is achieved for the best thermoelectric films. The agreement between the results of Raman and XRD analysis for films studied in this work and the values reported in literature for bulk  $\text{Bi}_2\text{Te}_3$  shows that the thin-film composition is close to stoichiometry. The narrow FWHM of both Raman and XRD peaks reveals an extensive crystalline phase in the  $\text{Bi}_2\text{Te}_3$  films.

The flexible electronics concept is demonstrated by the use of a  $25\text{ }\mu\text{m}$ -thick polyimide foil as substrate. Due to its low thermal

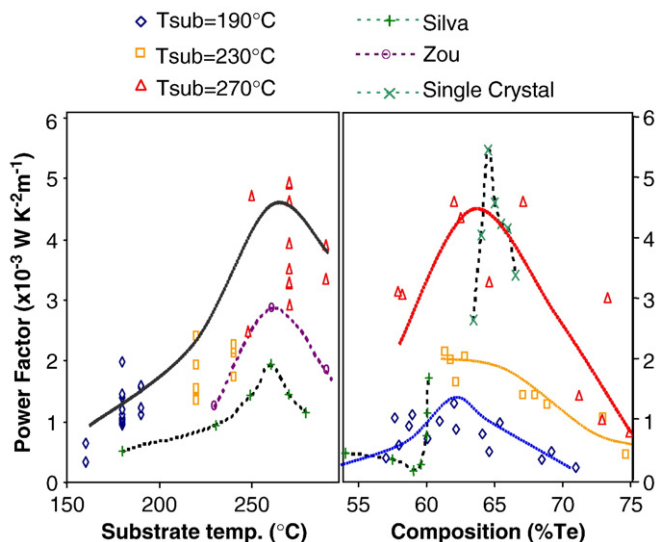


Fig. 6. Power factor of selected  $\text{Bi}_2\text{Te}_3$  films plotted as a function of substrate temperature (left) and as a function of composition, obtained by EDX (right). Lines are guides to the eye.

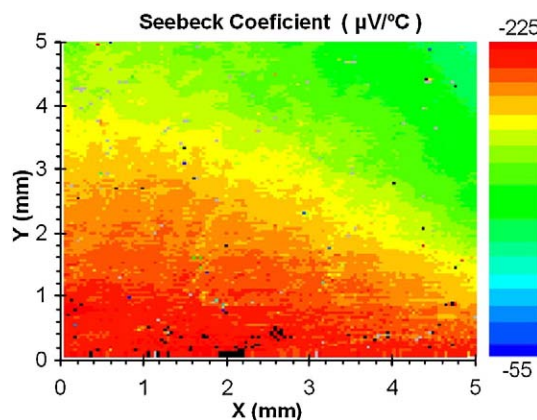


Fig. 7. Map of Seebeck coefficient distribution on a film surface: the small squares are the  $40\text{ }\mu\text{m} \times 40\text{ }\mu\text{m}$  spots where the Seebeck coefficient was evaluated.

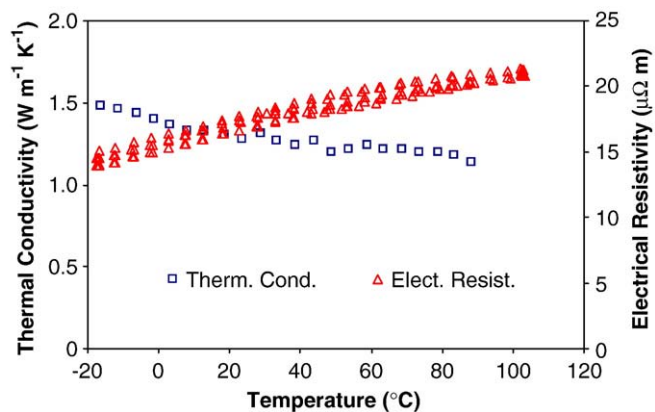


Fig. 8. Thermal conductivity and electrical resistivity of a  $\text{Bi}_2\text{Te}_3$  film, measured from  $-20^\circ\text{C}$  to  $100^\circ\text{C}$ .

conductivity and high upper working temperature, polyimide is an adequate choice for planar thermoelectric device fabrication. The thermoelectric properties achieved with  $\text{Bi}_2\text{Te}_3$  thin films deposited on polyimide in this work are suitable for the fabrication of Peltier micro-coolers and thermoelectric micro-generators [3].

#### Acknowledgements

The authors thank the Portuguese Foundation for Science and Technology and Adi for funding this work (SFRH/BD/18142/2004, FCT/PTDC/EEA-ENE/66855/2006 and MPYROM); D.M. Rowe and Gao Min (University of Cardiff) for guidelines; Stefano Chiussi (University of Vigo, Spain) for XPS analysis, Dieter Platzek (Panco GmbH, Germany) for Seebeck image map and David Barber (University of Essex) for

English amendments. We are also indebted to the Chemistry and Physics departments from University of Aveiro where the Raman scattering experiments were performed and Instituto Tecnológico e Nuclear for RBS/PIXE analysis.

#### References

- [1] Gao Min, D.M. Rowe, *Solid State Electron.* 43 (1999) 923.
- [2] G. Jeffrey Snyder, James R. Lim, Chen-Kou Huang, Jean-Pierre Fleurial, *Nat. Mater.* 2 (2003) 528.
- [3] L.M. Goncalves, J.G. Rocha, C. Couto, P. Alpuim, Gao. Min, D.M. Rowe, J.H. Correia, *J. Micromechanics Microengineering* 17 (2007) S168.
- [4] Helin Zou, D.M. Rowe, S.G.K. Williams, *Thin Solid Films* 408 (2002) 270.
- [5] Luciana W. da Silva, Massoud Kaviany, Citrad Uher, *J. Appl. Phys.* 97 (2005) 114903.
- [6] Ding-ho Kim, Eungsun Byon, Gun-Hwan Lee, Sunglae Cho, *Thin Solid Films* 510 (2006) 148.
- [7] Harald Böttner, Joachim Nurnus, Alexander Gavrikov, Gerd Kühner, Martin Jäggle, Christa Künzel, Dietmar Eberhard, Gerd Plescher, Axel Schubert, Karl-Heinz Schlereth, *J. Microelectromechanical Syst.* 3 (2004) 414.
- [8] Luciana W. da Silva, Massoud Kaviany, *J. Microelectromechanical Syst.* 14 (2005) 1110.
- [9] L.M. Goncalves, C. Couto, P. Alpuim, D.M. Rowe, J.H. Correia, *Sens. Actuators A* 130-131 (2006) 346.
- [10] W. Kullmann, J. Geurts, W. Richter, N. Lehner, H. Rauh, U. Steigenberger, G. Eichhorn, R. Geick, *Phys. Status Solidi B* 125 (1984) 131.
- [11] F. Völklein, H. Balles, *J. Microelectromechanical Syst.* 1 (1992) 193.
- [12] Powder Diffraction File, Joint Committee on Powder Diffraction Standards, ASTM, Philadelphia, PA, 1967.
- [13] M.A. Reis, L.C. Alves, *Nucl. Instrum. Methods Phys. Res., Sect. B* 68 (1992) 300.
- [14] J.O. Jenkins, J.A. Rayne, R.W. Ure, *Phys. Rev. B* 5 (1972) 3171.
- [15] W. Richter, H. Köhler, C.R. Becker, *Phys. Status Solidi (b)* 84 (1977) 619.
- [16] M. Cutler, N.F. Mott, *Phys. Rev.* 181 (1969) 1336.
- [17] H. Scherrer, S. Scherrer, in: D.M. Rowe (Ed.), *CRC handbook of thermoelectrics*, CRC Press, New York, 1995, p. 220.
- [18] D. Platzek, G. Karpinski, C. Stiewe, P. Ziolkowski, M. Stordeur, B. Engers, E. Müller, B. Lenoir, A. Dauscher, 3rd European Conf. Thermoelectrics, Nancy, France, 1–2 September 2005, *Proc. 3rd European Conf. Thermoelectrics*, 2005, p. 138.
- [19] Rama Venkatasubramanian, Edward Siivola, Thomas Colpitts, Brooks O'Quinn, *Nature* 413 (2001) 597.